FEM Simulation on Elastic Constants of Porous Silicon for Acoustic Propagation Investigation

X. Gong[a], J. Bustillo[b], L. Blanc[a] et G. Gautier[a]
[a]GREMAN UMR7347 CNRS, U.Tours, INSA-CVL, GREMAN, INSA-CVL 3 rue de la chocolaterie, 41000 Blois, France
[b]GREMAN UMR7347 CNRS, U.Tours, INSA-CVL, GREMAN site ST, 10 rue Thales de Milet, 37100 Tours, France
xiaoyue.gong@univ-tours.fr

Porous silicon seems to be a promising material for acoustic sensing due to its tunable properties and high capabilities. In addition, wave propagation in porous material is required to enhance the sensor sensitivity. According to Biot's theory, wave propagation is governed by the porous matrix modulus. These parameters are difficult to measure and are often estimated using ultrasonic measurements. Hence, FEM simulation method is choosed here to estimate the elastic parameters of porous silicon (*i.e.* Young's modulus) as a function of porosity. Then, the influence of pore morphology on elastic parameters is observed. The silicon substrate has a ⟨100⟩ crystallographic direction and the pores are cylinder-like. Five pore shapes are designed in order to investigate the influence of the morphology on elastic parameters. These shapes are chosen to be close to geometries obtained by electrochemical etching. It is shown that the morphology of the pores has a significant influence on elastic constants, even if the geometries are nearby. Finally, the simulation results are in good agreement with the literature for Young's modulus.

1 Introduction

As an artificial material whose morphology can easily be controlled during the manufacturing processdure, Porous Silicon (PSi) seems to be a very promising material in many areas, *e.g.* drug delivery [1], lithium battery [2], solar cells [3], micro-fuel cell [4], *etc.*. PSi could also be used in acoustic sensing due to its tunable properties, its integration in lab-on-chips systems and its high capabilities [5]. Yet, parameters such as sensitivity or working frequency are dependent on wave propagation in porous material [6, 7]. Therefore, according to Biot's theory on wave propagating in porous materials [8, 9], a good knowledge of the elastic parameters of PSi is needed.

Optical, electrical and thermal properties of PSi have been widely studied due to their numerous application fields [10]. But, elastic properties of PSi have also been studied by several researchers. Using X-Ray Diffraction, K. Barla *et al.* [11, 12] showed that the lattice constant of porous layer increases according to the porosity ϕ (the ratio between the volume of the pores and PSi). Young's modulus is directly related to lattice constants and so to pore structure. Da Fonseca *et al.* [13, 14] used acoustic microscopy to investigate PSi manufactured on p+-type (doping level $> 10^{18}\ cm^{-3}$) ⟨100⟩ crystalline silicon wafer. He described longitudinal and shear wave velocities V as functions of porosity, $V = V_0(1-\phi)^n$, where V_0 is the velocity in crystalline silicon and n is a fitting parameter. Measurements have shown the good agreement with theory using Da Fonseca formulas [15, 16]. Using transmission spectroscopy, G. N. Aliev [17] derived a semi-empirical relation of wave velocity and porosity which is the same as Fonseca's fitting formula, but with different fitting numbers. He assumed that the Poisson ratio of PSi ν_p is independent of porosity ϕ and identical to those of crystalline silicon. According to this assumption, Martini *et al.* [18] have studied mechanical properties of sintered mesoporous silicon using Finite Element Methods (FEM). He modeled porous silicon using randomly distributed spherical pores and concluded that properties of the sintered PSi are in good agreement with experiments.

D. Bellet *et al.* [19] applied nano-indentation technique on the investigation of Young's modulus in PSi with porosity rangeing from 36% to 90% and showed that the doping level has an influence on PSi Young's modulus. Yet, he also pointed out that the main difference between p+ and p-type PSi is the pore structure. By taking a constant PSi Poisson ratio ($\nu_p = 0.10$), Bellet concluded that p+-type ⟨100⟩ oriented PSi Young's modulus follows a power law function: $E_p = A(1-\phi)^2$, where $A = 120GPa$. By using the discrete homogenization apporach, Magoariec [20] gave the same function as Bellet. C. Populaire, *et al.* [21] proposed a new function for Young's modulus as: $E_p = E_0(1-\phi)^2$, where E_0 is Young's modulus of crystalline silicon.

The investigation methods discussed above have all obtained interested results, but limited by the assumption they have taken. Moreover, discrepancies are observed on similar results. Nevertheless, they give explanations on the microscopic mechanics of elastic parameters of PSi and they all mentioned that pore structure is a key factor to estimate elastic properties of PSi. Yet, the influence of these factors cannot be easily analytically studied or quantified by experiments.

Therefore, an investigation on the influence of the pore structure using FEM simulation is proposed in this article. Firstly, the theoretical background used for elastic parameters determination is presented. Secondly, the numerical simulations are performed on five different shapes, corresponding to common pore geometries. Finally the results of these simulations are presented and discussed.

2 Theoretical background

Since Biot had pointed out that elastic matrix is one of the key factors to acquire wave propagation in porous materials, it is thus important to figure out the way to obtain parameters being wanted.

Hooke's law gives the relationship between the stress σ applied to a medium to its strain $\mathbf{e}$ as:

$$\sigma = C\mathbf{e} \tag{1}$$

where C is the stiffness tensor. The number of independent parameters in this tensor depends on the symmetry of the material (from 2 for isotropic to 21 for triclinic crystal). In case of a material having axis-symmetric inclusions, the symmetry is chosen as orthotropic. In this case, the tensor has nine independent parameters and can be written as:

$$C = \begin{bmatrix} C_{11} & C_{12} & C_{13} & 0 & 0 & 0 \\ C_{12} & C_{22} & C_{23} & 0 & 0 & 0 \\ C_{13} & C_{23} & C_{33} & 0 & 0 & 0 \\ 0 & 0 & 0 & C_{44} & 0 & 0 \\ 0 & 0 & 0 & 0 & C_{55} & 0 \\ 0 & 0 & 0 & 0 & 0 & C_{66} \end{bmatrix} \tag{2}$$

In case of cubic symmetry, such as in crystalline silicon, only 3 parameters are independent due to the fact that $c_{12} = c_{13} = c_{23}$, $c_{11} = c_{22} = c_{33}$ and $c_{44} = c_{55} = c_{66}$. Using

equations (1) and (2), the elastic parameters on principle orientation of crystalline silicon can be deduced from the stiffness tensor like [17, 22]:

$$\begin{aligned} E_0 &= \tfrac{1}{2}\tfrac{(c_{11}-c_{12})(c_{11}+2c_{12})}{c_{11}+c_{12}} \\ \nu_0 &= \tfrac{c_{12}}{c_{11}+c_{12}} \\ G_0 &= c_{44} \\ K_0 &= \tfrac{c_{11}+2c_{12}}{3} \end{aligned} \tag{3}$$

where E_0 is the Young's modulus, ν_0 is the Poisson ratio, G_0 is the shear modulus and K_0 is the bulk modulus. The footnote "0" is used to denote the bulk material with no pore inside.

The Hooke's Law can also be rewritten as a strain-stress relationship:

$$\mathbf{e} = S\sigma \tag{4}$$

where S is the compliance tensor. This tensor is equal to the inverse of the stiffness tensor. This relationship is useful to estimate the mechanical parameters of an orthotropic medium because it is directly related to the Young's modulus E_i, Shear modulus, G_{ij} and Poisson ratio ν_{ij} in each direction:

$$\begin{bmatrix} e_x \\ e_y \\ e_z \\ \gamma_{yz} \\ \gamma_{zx} \\ \gamma_{xy} \end{bmatrix} = \begin{bmatrix} \frac{1}{E_x} & -\frac{\nu_{yx}}{E_y} & -\frac{\nu_{zx}}{E_z} & 0 & 0 & 0 \\ -\frac{\nu_{xy}}{E_x} & \frac{1}{E_y} & -\frac{\nu_{zy}}{E_z} & 0 & 0 & 0 \\ -\frac{\nu_{xz}}{E_x} & -\frac{\nu_{yz}}{E_y} & \frac{1}{E_z} & 0 & 0 & 0 \\ 0 & 0 & 0 & \frac{1}{G_{yz}} & 0 & 0 \\ 0 & 0 & 0 & 0 & \frac{1}{G_{zx}} & 0 \\ 0 & 0 & 0 & 0 & 0 & \frac{1}{G_{xy}} \end{bmatrix} \begin{bmatrix} \sigma_x \\ \sigma_y \\ \sigma_z \\ \tau_{yz} \\ \tau_{zx} \\ \tau_{xy} \end{bmatrix} \tag{5}$$

Therefore, elastic parameters can be deduced by applying each kind of load and observing the associated strains. As an example, by applying a normal stress σ_x on $yz-$ surface of porous medium, with free lateral faces, we have $e_x = \sigma_x/E_x$, $e_y = -(\sigma_x\nu_{xy})/E_x$, and $e_z = -(\sigma_x\nu_{xz})/E_x$. By inverting these formulas, the elastic parameters are deduced:

$$\begin{aligned} E_i &= \sigma_i/e_i \\ \nu_{ij} &= -e_j/e_i \\ G_{ij} &= \tau_{ij}/\gamma_{ij} \end{aligned} \tag{6}$$

Because of the axial symmetry of the pores, there exist the following relations: $E_y = E_z$; $\nu_{xy} = \nu_{xz}$, $\nu_{yx} = \nu_{zx}$, $\nu_{yz} = \nu_{zy}$.

By applying a hydrostatic pressure on the surface of the medium, *i.e.* $\sigma_x = \sigma_y = \sigma_z = p$, and shear stress $\tau_x = \tau_y = \tau_z = 0$. Then, $e_x = (\frac{1}{E_x} - \frac{\nu_{yx}}{E_y} - \frac{\nu_{zx}}{E_z})p$, $e_x = (\frac{1}{E_x} - \frac{\nu_{yx}}{E_y} - \frac{\nu_{zy}}{E_z})p$, $e_z = (\frac{1}{E_z} - \frac{\nu_{xz}}{E_x} - \frac{\nu_{yz}}{E_y})p$ and the bulk modulus for PSi K_b can be deduced:

$$K_b = \frac{p}{e_x + e_y + e_z} \tag{7}$$

which means that bulk modulus can be computed using hydrostatic pressure divided by volume decrement. Additionally, we can also calculate it from Young's modulus and Poisson ratio. According to the computing formulas (6) for elastic parameters of porous material, it is possible to use FEM simulation to observe the elastic behavior of materials, porous or not. Since the elastic properties of pure silicon have been well studied [23], PSi is treated as a bulk silicon with pores inside, and its elastic behaviors were thus observed in COMSOL Multiphysics®©. Different porosities were achieved by setting different pore size, pore distribution or distance between pores. By changing the shape of pores, the influence of pore structure on elastic parameters was also obtained.

3 Numerical simulations

Considering that PSi is etched from a ⟨100⟩ oriented silicon wafer, the simulated geometric model is set to be a cubic silicon with straight and periodically distributed pores along the x-coordinate. The components values of the stiffness tensor used for ⟨100⟩ oriented pure silicon can be found in previous work [24], as shown in Table 1.

Table 1: Values of stiffness components (in GPa) for Silicon at room temperature.

c_{11}	c_{12}	c_{44}
165.6	63.9	79.5

By using formulas (3), the elastic parameters for pure silicon are then calculated, and presented in Table 2.

Table 2: Values of the elastic parameters for Silicon at room temperature.

$E_0(GPa)$	ν_0	$G_0(GPa)$	$K_0(GPa)$
130	0.28	79.5	97.8

In order to lower the computational cost, the pores are set to be uniform and axisymmetric, thus, a cubic sample with only one pore in the middle is enough to be a representative volume element (RVE). Note that if the pore distribution is not uniform, one pore will not be enough to be considered as RVE. The side length of the cubic RVE is set at $a = 25nm$, as shown Figure 1. Yet, this dimension does not affect the simulation results and is only defined for COMSOL calculations. The pore is empty, *i.e.* without any materials, and the remaining part of the cube is pure silicon.

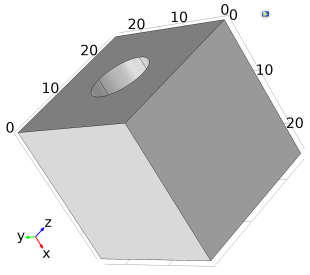

Figure 1: RVE of a PSi sample with cylindrical pores(scale in *nm*)

The elastic parameters of PSi are computed according to formulas (6). Thanks to the symmetries, periodic boundary conditions are set to decrease the computation cost, as shown in Figure 2 for Young's modulus. As for Young's modulus along other directions, it is simply a change of boundary conditions. It is the same for computing shear and bulk

modulus. After FEM computing, the displacement vector $\mathbf{u} = (u, v, w)$ and strain tensor $\mathbf{e}$ are obtained, as illustrated in Figure 3. Thus, according to formula (6), E_i, ν_{ji} and G_{ji} are all obtained. According to stress-strain relation (5), the compliance tensor of PSi S_{ij} is then obtained, as well as stiffness tensor C_{ij}.

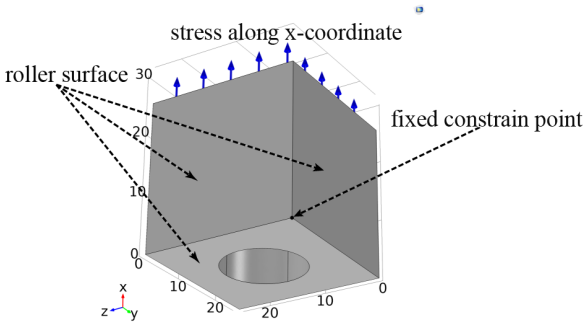

Figure 2: Description of boundary conditions for computing Young's modulus E_x

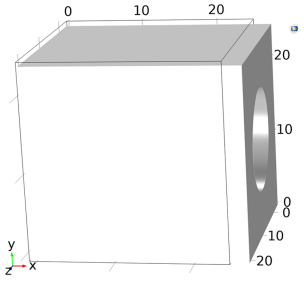

Figure 3: Deformation of PSi after being stretched on x-axis(scale in *nm*)

In fact, pores in PSi are not perfect cylinders, but present different morphologies depending on substrate properties and manufacturing process [25]. For example, it may be with varying radius, or with branches.

Thus, to expend the study range and obtain reliable results, several different kinds of pore morphology are used. Chosen pore shapes are shown in Figure 4, save the cylindrical reference. The studied crystalline orientation is ⟨100⟩ and the pore is along X-axis. Considering that p+- and p-type silicon will also change the pore shape, therefore doping level is not chosen as an influencing factor on mechanics, but using pore shapes instead. For one specified pore shape, different porosities are obtained by changing the size of the pore.

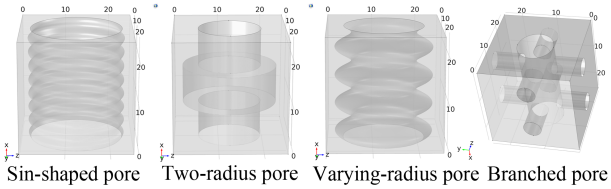

Figure 4: Different shapes of pores adapted in the FEM simulation.

4 Results and discussion

Figure 5 is the comparison between the FEM result of E_y of PSi with branched pore and the Young's modulus given by other researchers with different approaches. It seems that the FEM result and Magoariec's [20] numerical results using discrete homogenization approach are both close to D. Bellet's [19] using nanoindentation technique, but FEM result obviously has more conformity with it than the other numerical one.

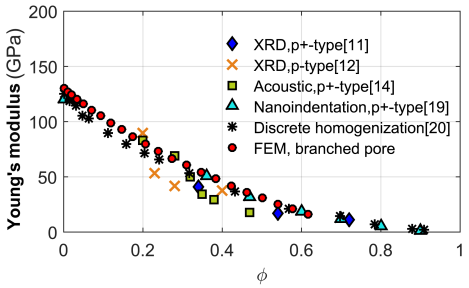

Figure 5: Young's modulus of PSi given by other research methods compare with FEM simulation in this article

The FEM results of Young's modulus for different shapes of pore are presented in Figure 6. The results of PSi with different shapes of pores are thus compared. Because of axial symmetry, E_z is the same as E_y.

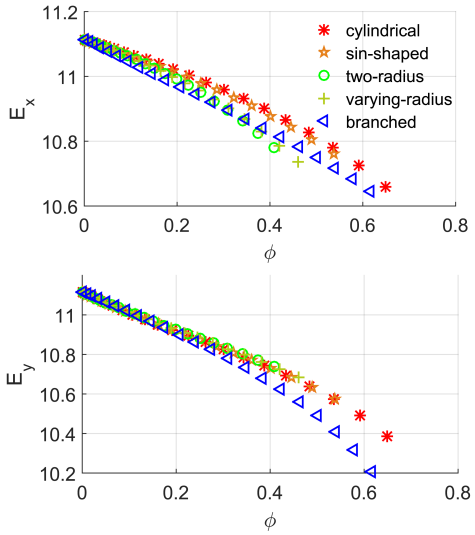

Figure 6: Comparison of Young's moduli belongs to PSi with different shapes of pores

The evolution of the elastic parameters (mainly Young's modulus) as a function of porosity clearly depends not only on porosity but also the pore geometry. Moreover, elastic parameters with the cylindrical and sin-shaped geometries are closely equal, so are the two-radius and varied-radius geometries. In fact, the radius does not drastically change between sin-shaped and cylindrical geometry whereas the two-radius pore and varied-radius geometry have huge variation of the radius on the x-axis direction. Finally, it can be noted that branches significantly affect Young's modulus of Y-axis. Fitting functions of Young's modulus E of PSi have been proposed by Martini [18] as a power law as:

$$E = E_0(1 - \phi)^m \tag{8}$$

where E_0 is the Young's modulus of crystalline silicon (equation (3)). m is fitting number who is in the range of $1.58504 \leq m \leq 2.47781$.

Using this formulation, the parameter m has been fitted on numerical values of the elastic parameters and given in Table 3 for the Young modulus.

Table 3: Fitting parameters of power law for Young's modulus

shape	$m(E_x)$	$m(E_y)$
cylindrical pore	1.0000	1.5782
sin-shaped pore	1.0543	1.6246
two-radius pore	1.4280	1.6615
varying-radius pore	1.3929	1.6244
branched pore	1.1373	2.1106

Values of fitting number m is close to the values given by Roberto Martini [18]. It can also be observed that the values for cylindrical and sin-shaped geometries are similar, whereas the two radius and the varying radius geometries are close. These results show that the cylindrical model is good enough if the radius modulation is low and two radius model has to be used if the modulation is high. On the other hand, the results for branched pore show that its behavior cannot be simply explained by a cylinder or a two radius model.

5 Conclusion

The influence of pore shape on elastic parameters as a function of porosity have been successfully studied using FEM simulation. From the analysis of simulation results and comparison with those from other literature, it can be concluded that: the shape of pore has significant effect on elastic properties of PSi, and when its porosity increases, elastic parameters decrease following power law. But there exist some simplifications on the pore shape, *i.e.* when there is only small variations on radius, its geometrical model can be simplified as cylinders, according to the FEM results; whereas when the variations of pore radius is too big to be ignored, it may be assumed as two-radius model; yet when there are branches on sides of the main pore, they can not be disregarded or simplified. These results have to be considered when building a geometrical model for real PSi.

Reference

[1] E. J. Anglin, L. Cheng, W. R. Freeman, and M. J. Sailor, "Porous silicon in drug delivery devices and materials," *Advanced Drug Delivery Reviews*, vol. 60, no. 11, pp. 1266–1277, 2008.

[2] Z. Lu, N. Liu, H. W. Lee, J. Zhao, W. Li, Y. Li, and Y. Cui, "Nonfilling Carbon Coating of Porous Silicon Micrometer-Sized Particles for High-Performance lithium battery anodes," *ACS Nano*, vol. 9, no. 3, pp. 2540–2547, 2015.

[3] J. H. Petermann, D. Zielke, J. Schmidt, F. Haase, E. G. Rojas, and R. Brendel, "19%-efficient and 43 μm-thick crystalline si solar cell from layer transfer using porous silicon," *Progress in Photovoltaics: Research and Applications*, vol. 20, no. 1, pp. 1–5, 2012.

[4] G. Gautier and S. Kouassi, "Integration of porous silicon in microfuel cells: a review," *International Journal of Energy Research*, vol. 39, pp. 1–25, jan 2015.

[5] G. S. Korotchenkov, *Porous silicon : from formation to application. Volume one. Formation and properties*. CRC Press, 2015.

[6] G. Tortissier, L. Blanc, A. Tetelin, C. Zimmermann, J.-L. Lachaud, C. Boissière, C. Sanchez, C. Déjous, and D. Rebière, "Mesoporous coated films on love wave acoustic devices for gas detection," *Sensor letters*, vol. 7, no. 5, pp. 984–988, 2009.

[7] I. Gammoudi, L. Blanc, F. Moroté, C. Grauby-Heywang, C. Boissière, R. Kalfat, D. Rebière, T. Cohen-Bouhacina, and C. Dejous, "High sensitive mesoporous TiO2-coated love wave device for heavy metal detection," *Biosensors and Bioelectronics*, vol. 57, pp. 162–170, 2014.

[8] M. A. Biot, "Theory of Propagation of Elastic Waves in a Fluid-Saturated Porous Solid. I. Low Frequency Range," *The Journal of the Acoustical Society of America*, vol. 28, no. 2, pp. 168–178, 1956.

[9] M. A. Biot, "Theory of Propagation of Elastic Waves in Fluid-Saturated Porous Solid. II. Higher frequency range," *The Journal of the Acoustical Society of America*, vol. 28, no. 2, pp. 179–191, 1956.

[10] L. Canham, *Handbook of Porous Silicon*. Springer, 2014 ed., 2014.

[11] K. Barla, R. Herino, G. Bomchil, J. C. Pfister, and A. Freund, "Determination of lattice parameter and elastic properties of porous silicon by X-ray diffraction," *Journal of Crystal Growth*, vol. 68, no. 3, pp. 727–732, 1984.

[12] R. S. Dariani and M. Nazari, "Comparison of stress, strain, and elastic properties for porous silicon layers supported by substrate and corresponding membranes," *Journal of Molecular Structure*, vol. 1119, pp. 308–313, 2016.

[13] R. J. M. Da Fonseca, J. M. Saurel, and G. Despaux, "Elastic characterization of porous silicon by acoustic microscopy," *Superlattices and Microstructures*, no. July, pp. 21–23, 1994.

[14] R. J. M. Da Fonseca, J. M. Saurel, A. Foucaran, J. Camassel, E. Massone, T. Taliercio, and Y. Boumaiza, "Acoustic investigation of porous silicon layers," *Journal of Materials Science*, vol. 30, no. 1, pp. 35–39, 1995.

[15] J. Bustillo, J. Fortineau, G. Gautier, and M. Lethiecq, "Ultrasonic characterization of electrochemically etched porous silicon," *Japanese Journal of Applied Physics*, vol. 53, no. 6, pp. 1–4, 2014.

[16] J. Bustillo, J. Fortineau, G. Gautier, and M. Lethiecq, "Ultrasonic characterization of porous silicon using a genetic algorithm to solve the inverse problem," *NDT and E International*, vol. 62, pp. 93–98, 2014.

[17] G. N. Aliev, B. Goller, and P. A. Snow, "Elastic properties of porous silicon studied by acoustic transmission spectroscopy," *Journal of Applied Physics*, vol. 110, no. 4, pp. 1–8, 2011.

[18] R. Martini, V. Depauw, M. Gonzalez, K. Vanstreels, K. V. Nieuwenhuysen, I. Gordon, and J. Poortmans, "Mechanical properties of sintered meso-porous silicon: a numerical model," *Nanoscale Research Letters*, vol. 7, no. 1, p. 597, 2012.

[19] D. Bellet, P. Lamagnère, A. Vincent, and Y. Bréchet, "Nanoindentation investigation of the Young's modulus of porous silicon," *Journal of Applied Physics*, vol. 80, no. 7, pp. 3772–3776, 1996.

[20] H. Magoariec and A. Danescu, "Modeling macroscopic elasticity of porous silicon," *Physica Status Solidi (C) Current Topics in Solid State Physics*, vol. 6, no. 7, pp. 1680–1684, 2009.

[21] C. Populaire, B. Remaki, V. Lysenko, D. Barbier, H. Artmann, and T. Pannek, "On mechanical properties of nanostructured meso-porous silicon," *Applied Physics Letters*, vol. 83, no. 7, pp. 1370–1372, 2003.

[22] H. J. McSkimin and P. Andreatch, "Elastic moduli of silicon vs hydrostatic pressure at 25.0°C and -195.8°C," *Journal of Applied Physics*, vol. 35, no. 7, pp. 2161–2165, 1964.

[23] M. A. Hopcroft, W. D. Nix, and T. W. Kenny, "What is the Young's Modulus of Silicon?," *Journal of Microelctromechanical Systems*, vol. 19, no. 2, pp. 229–238, 2010.

[24] J. J. Hall, "Electronic effects in the elastic constants of *n*-type silicon," *Phys. Rev.*, vol. 161, pp. 756–761, Sep 1967.

[25] H. Föll, M. Christophersen, J. Carstensen, and G. Hasse, "Formation and application of porous silicon," *Materials Science and Engineering: R: Reports*, vol. 39, no. 4, pp. 93–141, 2002.